Hydrodynamics in curved membranes: The effect of geometry on particulate mobility

Mark L. Henle[1] and Alex J. Levine[2,3]
[1]*School of Engineering and Applied Sciences, Harvard University, Cambridge, Massachusetts 02138, USA*
[2]*Department of Chemistry and Biochemistry, University of California, Los Angeles, California 90095, USA*
[3]*California Nanosystems Institute, University of California, Los Angeles, California 90095, USA*
(Received 17 November 2009; published 12 January 2010)

We determine the particulate transport properties of fluid membranes with nontrivial geometries that are surrounded by viscous Newtonian solvents. Previously, this problem in membrane hydrodynamics was discussed for the case of flat membranes by Saffman and Delbrück [P. G. Saffman and M. Delbrück, Proc. Natl. Acad. Sci. U.S.A. **72**, 3111 (1975)]. We review and develop the formalism necessary to consider the hydrodynamics of membranes with arbitrary curvature and show that the effect of *local* geometry is twofold. First, local Gaussian curvature introduces in-plane viscous stresses even for situations in which the velocity field is coordinate-independent. Secondly, even in the absence of Gaussian curvature, the geometry of the membrane modifies the momentum transport between the bulk fluids and the membrane. We illustrate these effects by examining in detail the mobilities of particles bound to spherical and cylindrical membranes. These two examples provide experimentally testable predictions for particulate mobilities and membrane velocity fields on giant unilamellar vesicles and membrane tethers. Finally, we use the examples of spherical and cylindrical membranes to demonstrate how the *global* geometry and topology of the membrane influences the membrane velocities and the particle mobilities.

DOI: 10.1103/PhysRevE.81.011905 PACS number(s): 87.16.dp, 68.05.−n

I. INTRODUCTION

The dynamics of particles embedded in viscous fluid membranes underlies a number of fundamental biological processes involving the kinetics of proteins [1], lipid rafts [2], and lipid domains [3] in membranes. Cell-cell signaling, membrane-cytoskeleton interactions, and viral entry into cells provide three broad classes of biophysical dynamical systems whose underlying physics depends on the transport properties of lipid membranes. The dynamics of particles trapped at decorated fluid interfaces such as Langmuir monolayers [4–7] or liquid-liquid interfaces [8], as well as the motion of lipid domains on giant unilamellar vesicles [9], provide nonbiological systems in which membrane hydrodynamics plays a crucial role. Additional examples of such systems include the kinetics of colloids on liquid droplets during the formation of colloidosomes [10] and even the dynamics of polymers adsorbed on a fluid membrane [11].

To study these dynamics, one must understand the hydrodynamics of membrane flows. In this problem, one commonly approximates the membrane as two-dimensional (2D) viscous liquid surrounded above and below by three-dimensional (3D) ones [4,5,12–14,18], referred to hereafter as the *embedding fluids*. This approximation is valid for films thin enough that their velocity field gradients in the direction normal to the film are vanishingly small [15]. We work exclusively in this limit. Moreover, we specialize to the common case of membranes that are incompressible and impermeable to the embedding liquids.

The embedding liquids are coupled to the fluid membrane by the usual stick and stress balance boundary conditions. The stick boundary conditions require the velocity of the embedding liquids at the surface of the membrane to be equal to the membrane fluid velocity. In this work, we study only tangential flows in the membrane (i.e., ones that do not change the membrane geometry) and thus set the normal velocities to zero on the membrane. Unlike a simple liquid-liquid interface, the two-dimensional membrane is a distinct fluid. As a result, the membrane can exert and support stresses, so that the stress balance condition can lead to a stress discontinuity between the embedding liquids across the membrane surface.

The ability of the membrane to support stresses is what distinguishes membrane hydrodynamics from other problems in low Reynolds number hydrodynamics. Normally, in the inertia-free limit, hydrodynamics becomes a scale-free theory. The analogous low Reynolds number hydrodynamics problem in a membrane, however, contains a new length scale set by the ratio of the membrane viscosity η_m to the viscosity η of the embedding liquid. From dimensional analysis, one sees that their ratio is a length; In deference to the pioneering work by Saffman and Delbrück [12,16] we refer to $\ell_0 = \eta_m / \eta$ as the Saffman-Delbrück (SD) length. Physically, it sets the scale over which in-plane momentum in the membrane is dissipated by the embedding fluid.

Given that membrane hydrodynamics has an intrinsic length scale, one may ask how ask that length interacts with other length scales in determining the flows induced by the motion of membrane-embedded objects. One obvious candidate is the spatial extent of the object itself. Another is the length introduced by the local geometry of the membrane—the local radius of curvature. Here, we restrict our analysis to pointlike objects to focus on the latter. The mobility of extended objects [8,17] can be studied in terms of a collection of pointlike ones using the linearity of the hydrodynamic equations [14,18]. Previous work on the mobility of particles on a spherical membrane showed that curvature leads to dramatic changes in particle mobility when the radius of the membrane R is at least comparable to the SD length ℓ_0 [8,19]. In this article, we extend our previous work to study the effect of more general membrane geometries on particle

mobilities and membrane fluid flows in response to particulate transport. We rederive the membrane hydrodynamics equations in their most general covariant form, which allows us to study the hydrodynamics of membranes of arbitrary geometry. We also discuss the coupling of this system to the embedding fluid. Using these results we specialize to two particular membrane geometries: spherical and cylindrical membranes. These two cases were chosen since both have spatially constant curvature, greatly simplifying the solution of the hydrodynamic equations of the membrane. Moreover, since the Stokes equation can be readily solved in both spherical and cylindrical coordinates, we are able to provide complete analytic solutions for the full problem of the coupled flows of the membrane and the embedding fluid. The comparison of these two cases with each other and with the better known result for a flat membrane allows us to investigate the differing effects of mean and Gaussian curvature on particulate mobility and membrane flows.

The comparison of flows on the sphere and the cylinder also brings to light a dynamical difference that is of a fundamentally topological nature by showing how the Euler characteristic of the surface affects the structure of the flows on the membrane. On a sphere, the continuous fluid velocity vector field is required to contain at least two singularities [20] in the form of sources, sinks, or vortices. For an incompressible membrane, only vortices are permitted. Cylindrical and flat membranes, having a different Euler characteristic, require no such singularities. We return to this point later in the discussion of our results.

Throughout this article, we treat both the membrane and the embedding fluids as Newtonian. There are numerous examples of non-Newtonian (i.e., viscoelastic) effects [21,22] and nonlinear flow effects [23] in membrane dynamics both in Langmuir monolayers and in composite, biomimetic membranes [24,25]. By working in the frequency domain, the results presented below can be readily generalized to such cases [13]. Finally, we only consider membranes whose particulate concentrations are low enough that their presence does not affect the viscosities of either the membrane or the embedding fluids; we have considered the effects of particle concentration on these viscosities to linear order in flat membranes previously [25,26].

The remainder of the paper is organized as follows: in Sec. II, we derive the equations of membrane hydrodynamics for an *arbitrarily curved* and incompressible membrane. Using these equations, we find the eigenvalue equation that determines the linearly independent in-plane modes of the membrane. For surfaces with a constant Gaussian curvature, the eigenvalue equation simplifies greatly. In Sec. III, we consider the coupling of an arbitrarily curved membrane to the embedding fluids that surround it. In Secs. IV and V, we consider the two simplest nonplanar membrane geometries: spheres and cylinders. In each of these sections, we find the membrane modes, solve the bulk Stokes equation, and determine the response of the system to a point force in the membrane. We then use the point-force response to investigate the mobility of particles embedded in these membranes.

In this article, we present many of the technical details of our calculation. For the reader more interested in the principal results and their interpretation, we collect these remarks in Sec. VI; We also discuss experimental tests of our results and open questions in membrane hydrodynamics there. For this reason we reserve the bulk of our discussion of the implications and meaning of our results for this section while presenting the mathematical formalism and quantitative results earlier.

II. STOKES EQUATION FOR A CURVED MEMBRANE; HYDRODYNAMICS MODES

To derive the Stokes equation for a curved membrane, we use the same underlying principles of mass and momentum conservation used to derive the Stokes equation for a bulk fluid or a flat 2D membrane. The problem of accounting for local membrane geometry when discussing the dynamics or statistical physics of curved membranes [27–29] and lamellar stacks of such membranes [30,31] has been well-studied. Thus, the application of differential geometry to the problem of integrating over membrane configurations (to address the statistics of membrane fluctuations) or of determining the relation between the local rate of stain and the stresses in the membrane has been developed. For completeness, we briefly recount these results here before turning to the problem of particle mobilities in the membrane.

In order to account for the curvature of the membrane, it is convenient to express these conservation laws in a *manifestly covariant* form. That is, the components of the membrane fluid velocity vector $\vec{v}$ are written in terms of either its covariant or contravariant: v_α and v^α, respectively. The partial derivatives ∂_α are replaced by covariant derivatives D_α. Here and throughout this article, we use Greek indices α, β, etc. exclusively to indicate in-plane components of the covariant vectors and tensors. One must use care in distinguishing the covariant and contravariant velocity vectors from the *physical* velocity vectors. For instance, the dimensions of v_α and v^α differ from each other and from the usual dimensions of velocity. To avoid confusion in using these results to fit data, we give the final expressions for the velocity field as *physical* velocity vectors distinguished by the notation $\vec{v}$.

We begin with the statement of mass conservation. A change in fluid density in any area patch A on the membrane must be due to fluid flow through the boundary curve C of that patch. In its covariant form, this statement is written as

$$\frac{\partial}{\partial t}\int_A \rho dA + \oint_C \rho v_\alpha n^\alpha ds = 0, \tag{1}$$

where ρ is the membrane fluid density and n_α is the outward normal to the curve C. In Eq. (1) and hereafter, we employ the Einstein summation convention, where repeated indices (one raised, one lowered) are summed. Using the two-dimensional divergence theorem [32], $\oint B_\alpha n^\alpha ds = \int D^\alpha B_\alpha dA$, we can convert Eq. (1) to a local statement,

$$\frac{\partial \rho}{\partial t} + D^\alpha[\rho v_\alpha] = 0. \tag{2}$$

Similarly, we can write the covariant integral statement of momentum conservation and use the 2D divergence theorem to convert this to a local statement. At low Reynolds number,

we can drop the inertial term, so that the local statement of momentum conservation is given by

$$D^{\beta}\Pi_{\alpha\beta} = 0, \tag{3}$$

where $\Pi_{\alpha\beta}$ is the momentum current tensor. In this section, we focus on isolated membranes; the stress exerted on the membrane by any surrounding fluids, as well as the response to externally applied stresses, will be taken into account in the next section by including these stresses in Eq. (3).

For a flat membrane, the covariant derivatives are equivalent to simple partial derivatives, $D_{\alpha}=D^{\alpha}=\partial_{\alpha}$, so that Eqs. (2) and (3) become the familiar statements of mass and momentum conservation. Indeed, these equations follow directly from the flat-space equations: they are the only way to generalize the flat-space equations to account for the locally varying geometry of an arbitrarily shaped membrane. If we generalize the usual expression for the momentum current tensor in the same fashion,

$$\Pi_{\alpha\beta} = pa_{\alpha\beta} - \eta_{\alpha\beta\mu\gamma}D^{\mu}v^{\gamma}, \tag{4}$$

where p is the membrane pressure, $\eta_{\alpha\beta\mu\gamma}$ is the viscosity tensor, and $a_{\alpha\beta}$ is the *metric tensor* for the surface. We have dropped the inertial term $\rho v_{\alpha}v_{\beta}$ from Eq. (4), because we assume the Reynolds number for the membrane is small. For a flat membrane or 3D fluid, the pressure term in the momentum current is proportional to the Kronecker delta function $\delta_{\alpha\beta}$. However, $\delta_{\alpha\beta}$ is not a covariant tensor, so for a curved membrane, it must be replaced by its covariant generalization $a_{\alpha\beta}$ (for a flat membrane, $a_{\alpha\beta}=\delta_{\alpha\beta}$).

For a flat isotropic membrane, the viscosity tensor $\eta_{\alpha\beta\mu\gamma}$ must be constructed entirely out of combinations of Kronecker delta functions. For a curved isotropic membrane, then, this tensor must be constructed entirely out of its metric tensors. Using the fact that the dissipative contribution to the momentum current must vanish for uniform velocities and uniform rotations, we find that the most general form of the viscosity tensor for an isotropic membrane is

$$\eta_{\alpha\beta\mu\gamma} = \eta_{\mathrm{m}}[a_{\alpha\mu}a_{\gamma\beta} + a_{\alpha\gamma}a_{\mu\beta}] + (\zeta_{\mathrm{m}} - \eta_{\mathrm{m}})a_{\alpha\beta}a_{\mu\gamma}, \tag{5}$$

where η_{m} and ζ_{m} are the shear and dilational (or bulk) viscosities, respectively. Hereafter, we insist on the incompressibility of the membrane—in other words, we require the membrane density to be constant in time and space. As a result, the mass conservation equation (2) implies that the velocity field is divergence free at all points $\vec{x}$ in the membrane,

$$D^{\alpha}v_{\alpha}(\vec{x}) = 0. \tag{6}$$

With this constraint, the dilational viscosity introduced in Eq. (5) becomes irrelevant and momentum transport within the membrane depends only on the remaining membrane viscosity η_{m}. The combination of incompressibility and momentum conservation expressed in Eqs. (4)–(6) generates the Stokes equation for the membrane fluid,

$$\eta_{\mathrm{m}}[D^{\beta}D_{\beta}v_{\alpha}(\vec{x}) + D^{\beta}D_{\alpha}v_{\beta}(\vec{x})] = D_{\alpha}p(\vec{x}). \tag{7}$$

The pressure in the membrane appearing on the right hand side of Eq. (7) must now be considered to be a Lagrange multiplier field; it acts as the constraint necessary to enforce membrane incompressibility as expressed by Eq. (6). If one were to allow for membrane compression, an equation of state for the membrane would be necessary to determine the fluid velocity and pressure field in the membrane.

For a flat membrane, the covariant derivatives—which reduce to simple partial derivatives—clearly commute with one another. In this case, the second term of Eq. (7) vanishes for incompressible membranes. This is not the case for covariant derivatives of a vector on a curved surface, i.e., $D_{\alpha}D_{\beta}v_{\mu} \neq D_{\beta}D_{\alpha}v_{\mu}$. In particular, it is straightforward to show that curvature implies the noncommutativity of the covariant derivatives [32,33]. Specifically, for an arbitrary vector field $w_{\beta}(\vec{x})$ in the two-dimensional manifold of the fluid membrane,

$$[D^{\beta}, D_{\alpha}]w_{\beta}(\vec{x}) = K(\vec{x})w_{\alpha}(\vec{x}), \tag{8}$$

where $K(\vec{x})$ is the local Gaussian curvature at the point $\vec{x}$ on the membrane. The interested reader may consult any text on basic differential geometry [32,33] for further details.

We can use Eqs. (6) and (8) to simplify Eq. (7),

$$\eta_{\mathrm{m}}[\Delta v_{\alpha}(\vec{x}) + K(\vec{x})v_{\alpha}(\vec{x})] = D_{\alpha}p(\vec{x}), \tag{9}$$

where $\Delta \equiv D^{\beta}D_{\beta}$ is the in-plane Laplacian operator acting on the membrane. This is the Stokes equation for an isolated membrane of arbitrary curvature. It clearly reduces to the flat membrane result, $\eta_{\mathrm{m}}\Delta\vec{v} = \vec{\nabla}_{\perp}p$, since the Gaussian curvature $K=0$ for a plane (here, $\vec{\nabla}_{\perp}$ is the 2D gradient for the plane).

In general, the hydrodynamic modes of a membrane consist of shear, compression, and bending deformations. In our system, the latter two modes are excluded by assumption as discussed in the introduction. The membrane velocity is thus composed entirely of shear modes. These modes are eigenmodes of the velocity-dependent terms in the Stokes equation (9). In general, there will be several eigenmodes $v_{\alpha}(\vec{x};s)$ with eigenvalues λ_s, so we write the eigenvalue equation as

$$\eta_{\mathrm{m}}[\Delta v_{\alpha}(\vec{x};s) + K(\vec{x})v_{\alpha}(\vec{x};s)] = \lambda_s v_{\alpha}(\vec{x};s). \tag{10}$$

All of these modes must also satisfy the incompressibility constraint, Eq. (6). We can automatically enforce this constraint by writing the shear modes as the antisymmetric derivative of a scalar function,

$$v_{\alpha}(\vec{x};s) = \epsilon_{\alpha\gamma}D^{\gamma}\Phi(\vec{x};s), \tag{11}$$

where $\epsilon_{\alpha\gamma}$ is an antisymmetric tensor defined in terms of the Levi-Civita tensor $e_{\alpha\gamma}$ by $\epsilon_{\alpha\gamma} = \sqrt{\det a}\, e_{\alpha\gamma}$. We can use this complete set of eigenmodes as a basis from which we can construct any membrane velocity field

$$v_{\alpha}(\vec{x}) = \sum_{s} A_s v_{\alpha}(\vec{x};s) = \sum_{s} A_s \epsilon_{\alpha\gamma}D^{\gamma}\Phi(\vec{x};s). \tag{12}$$

Using Eqs. (8) and (11), we can write Eq. (10) as

$$\eta_{\mathrm{m}}[D^{\gamma}\Delta\Phi + 2K(\vec{x})D^{\gamma}\Phi] = \lambda_s D^{\gamma}\Phi. \tag{13}$$

For the general case of a membrane with locally varying Gaussian curvature, this third-order differential eigenvalue equation is quite challenging to solve analytically. We expect that for many geometries it must be solved numerically, but there are dramatic simplifications for cases of constant

Gaussian curvature. The spherical and cylindrical membranes studied in Secs. IV and V (in addition to planar membranes, where $K=0$ everywhere) do have constant Gaussian curvature, rendering them analytically tractable. In these cases, Eq. (13) simplifies to

$$\Delta\Phi(\vec{x};s) = \left[\frac{\lambda_s}{\eta_m} - 2K\right]\Phi(\vec{x};s). \tag{14}$$

The eigenfunctions $\Phi(\vec{x};s)$ are clearly the eigenfunctions of the Laplacian on the membrane surface. For spheres, cylinders, and planes, these are well-known (see below for the cases of spheres and cylinders). The shear modes and the corresponding eigenvalues λ_s for the membrane follow directly from these modes.

III. POINT-FORCE RESPONSE OF THE COMBINED MEMBRANE/EMBEDDING FLUIDS SYSTEM

In the previous section, we considered the velocity modes of an *isolated* membrane. In physical systems of interest, the membrane is coupled to the embedding fluids that surround it. We treat these embedding fluids as incompressible Newtonian fluids whose hydrodynamics can be described by a three-dimensional, incompressible Stokes equation

$$\eta_\pm \vec{\nabla}^2 \vec{v}^\pm = \vec{\nabla} p^\pm, \quad \vec{\nabla}\cdot\vec{v}^\pm = 0. \tag{15}$$

Here, $\eta_\pm$, $\vec{v}^\pm$, and $p^\pm$ are the embedding fluid viscosities, velocities, and pressures, respectively, on either side of the membrane. For spherical and cylindrical membranes, the "+" ("−") superscript denotes the fluid on the exterior (interior) of the membrane. The coupling of the flows of the membrane to the flows in the embedding fluids is enforced by the boundary conditions at the surface of the membrane: the stick boundary conditions enforce continuity of the velocity across the membrane, while the stress-balance conditions account for the transmission of stresses between the embedding fluids and the membrane.

We can express the stick and stress-balance boundary conditions for an arbitrary membrane using the *normal coordinates* for the membrane. These Euclidean coordinates (u^1,u^2,u^3) are given by the 2D surface coordinates of the membrane (u^1,u^2), along with the distance u^3 away from the membrane surface, measured along the local membrane normal. For spherical and cylindrical membranes of radius R, the normal coordinates are simply the three-dimensional spherical and cylindrical coordinates, respectively, with $u^3=r-R$. For an arbitrary surface, these coordinates can always be defined close to the surface. In normal coordinates, the stick boundary conditions are

$$v_i^\pm(u^1,u^2,0) = v_i(u^1,u^2). \tag{16}$$

By assumption, the membrane velocity in the direction along its normal vanishes, $v_3(u^1,u^2)=0$. Using this and Eqs. (6) and (12), we can re-express the stick boundary conditions Eq. (16) in a more useful form,

$$v_3^\pm(u^1,u^2,0) = 0, \quad D^\alpha v_\alpha^\pm(u^1,u^2,0) = 0, \tag{17}$$

$$\epsilon^{\alpha\gamma} D_\gamma v_\alpha^\pm(u^1,u^2,0) = \sum_s A_s \Delta\Phi(\vec{x};s). \tag{18}$$

For surfaces of constant Gaussian curvature, the Laplacian $\Delta\Phi$ in Eq. (18) is given by Eq. (14).

In addition to the stick boundary conditions at the membrane surface, we also require that the embedding fluid velocities vanish at infinity and remain finite everywhere. Furthermore, we note that by writing the membrane velocity as a combination of shear modes, Eq. (11), we have implicitly excluded the possibility of the uniform translation of the membrane. Since we are interested in the mobility of objects embedded *within* the membrane and not the mobility of the entire membrane through the embedding fluids, this choice of boundary conditions is appropriate.

The final boundary conditions for this system are given by the in-plane stress-balance conditions at the membrane surface. For an isolated membrane, these are given by the Stokes equation (9). For the membrane/embedding fluids system, however, the flows in the embedding fluids exert stresses on the membrane that appear as externally generated force densities (i.e., forces per unit area) in the stress-balance condition. To calculate the response of the system to the motion of a particle embedded in the membrane, we also include one more externally applied stress that is the force per unit area applied directly to that particle. Taking these external stresses into account, the in-plane stress-balance conditions become

$$\sigma_\alpha^{\text{ext}} = -\sum_s \lambda_s A_s \epsilon_{\alpha\gamma} D^\gamma \Phi(\vec{x};s) + D_\alpha \Pi + [\sigma_{\alpha 3}^- - \sigma_{\alpha 3}^+]|_{u^3=0}, \tag{19}$$

where the bulk fluid stress tensor

$$\sigma_{ij}^\pm = \eta_\pm [D_i v_j^\pm + D_j v_i^\pm] - g_{ij} p_\pm, \tag{20}$$

where g_{ij} is the 3D metric tensor for the normal coordinates. We note that the components $T_{\alpha 3}$ of a tensor in 3D normal coordinates transforms as a 2D covariant *vector* on the surface $u^3=0$, so Eq. (19) is the covariant version of stress continuity across the membrane which accounts for the transfer of momentum between the membrane and the embedding fluids.

The stick boundary conditions Eqs. (17) and (18) can be used to solve for the embedding fluid velocities and stresses in terms of the amplitudes A_s of the membrane velocity shear modes. We can eliminate the membrane pressure Π from Eq. (19) by taking the antisymmetric derivative of this equation,

$$\epsilon^{\alpha\beta} D_\beta \sigma_\alpha^{\text{ext}} = -\sum_s \lambda_s A_s \Delta\Phi(\vec{x};s) + \epsilon^{\alpha\beta} D_\beta [\sigma_{\alpha 3}^- - \sigma_{\alpha 3}^+]|_{u^3=0}. \tag{21}$$

Once we have solved for the amplitudes A_s of the shear modes, the membrane pressure can be found by taking the symmetric derivative of Eq. (19). However, we will forgo this calculation for brevity, since our focus is on the membrane velocity and particle mobility.

We will assume throughout this paper that the radius a of the particle embedded in the membrane is much smaller than all other length scales in the problem, specifically the membrane size and the Saffman-Delbrück length. In this case, we can approximate the stress $\sigma_\alpha^{\text{ext}}$ caused by the force $\vec{F}_0$ acting on the particle by a point stress

$$\sigma_\alpha^{\text{ext}} = F_{0,\alpha}\delta^{(2)}(\vec{u}-\vec{u}_0), \tag{22}$$

where $\delta^{(2)}(\vec{u}-\vec{u}_0)$ is the appropriate Dirac delta function for the surface and $\vec{u}_0$ is the location of the particle. This point-stress approximation is valid for many of the situations in which particle mobilities are experimentally measured as well as the most common biophysical applications of our work. We can also employ this procedure when studying extended objects with a large aspect ratio using linear superposition [8,14,18]. For large circular membrane inclusions, the calculation must presumably proceed in terms of solving dual integral equations as done by Hughes *et al.* [34] and others [26].

The final step in our analysis is the computation of the particle mobility. Due to the linearity of the Stokes equation, the particle velocity—i.e., the velocity of the membrane at the location of the point force—must be parallel to the point force itself. The proportionality constant between the force and velocity is the particle mobility μ,

$$\lim_{\vec{u}\to\vec{u}_0} v_\alpha(\vec{u}) = \mu F_{0,\alpha}. \tag{23}$$

Given our point-force representation Eq. (22) of the stress in the membrane induced by the motion of the particle, we are confronted by logarithmic divergences in the particle mobility at short distances. This is due to the short-distance logarithmic behavior of the inverse Laplacian in two dimensions. As was recognized originally by Saffman and Delbrück, the coupling to the embedding fluids regularizes the similar logarithmic behavior at long distances. This allows for the definition of an intrinsic particle mobility—i.e., one that does not depend on the area of the membrane—but does nothing to fix the similar issue at short distances. Instead, the size a of the (rigid) particle prevents the short-distance divergence. We handle this divergence by cutting off the mode spectrum at a wave number proportional to $1/a$. This procedure has been shown to correctly reproduce the SD calculation of particulate mobilities for flat membranes [13].

IV. SPHERICAL MEMBRANES

We now specialize to the case of a spherical membrane of radius R. We follow the program discussed above of first determining shear modes of the membrane for this geometry, then solving the Stokes equations for the interior and exterior embedding fluids before finding the coupled modes of the membrane and embedding fluids linked by the stick and stress-balance boundary conditions. We then use the complete mode spectrum to calculate the response of the system to a tangential point force applied to the membrane. We focus on two results of this calculation. First, we study the membrane velocity and show how the radius of curvature and the topology of the sphere affects this velocity. Second, this calculation (when properly regularized at short distances) provides the mobility of a point particle on a spherical membrane. We examine this result for various values of the ratio of the sphere's radius to the SD length.

A. Membrane modes

For a sphere of radius R, the Gaussian curvature $K=1/R^2$ is constant. As shown in Sec. II, this implies that the shear eigenmodes for a spherical membrane can be found from the eigenmodes of the in-plane Laplacian, which is given by the angular components of the Laplacian in spherical coordinates. The eigenfunctions of this operator are the well-known spherical harmonics $Y_{l,n}(\theta,\phi)$. Then the shear eigenfunctions of the membrane are $\Phi(\vec{x};s)=Y_{l,n}(\theta,\phi)$ and these satisfy the equation

$$\Delta\Phi(\vec{x};s) = -\frac{l(l+1)}{R^2}\Phi(\vec{x};s). \tag{24}$$

From Eq. (14), we find that the eigenvalues λ_l, indexed by the angular momentum l, are

$$\lambda_l = \frac{\eta_{\text{m}}}{R^2}[2-l(l+1)], \tag{25}$$

and the membrane velocity field Eq. (12) expanded in terms of these eigenfunctions is

$$v_\alpha(\theta,\phi) = \sum_{l,n} A_{l,n}\epsilon_{\alpha\gamma}D^\gamma[Y_{l,n}(\theta,\phi)], \tag{26}$$

where the sums over the angular momentum and azimuthal indices l,n take the usual form: $\Sigma_{l,n}\equiv\Sigma_{l=1}^{\infty}\Sigma_{n=-l}^{l}$. The $l=0$ term does not contribute to this expression, since the spherical harmonic $Y_{0,0}$ is a constant, so we can exclude it from these sums.

B. Solution to the 3D Stokes equation

The general solution to the 3D Stokes equation (15) in spherical coordinates can be divided into two parts. The first part $\vec{v}^-$ is finite at the origin, and thus is suitable for the fluid velocity in the interior of the membrane. This solution can be written as $\vec{v}^-=\Sigma_{l=1}^{\infty}\vec{v}_l^-$, where [35]

$$\vec{v}_l^-(r,\theta,\phi) = \vec{\nabla}\times(\vec{r}q_l^-) + \vec{\nabla}w_l^- + \frac{1}{\eta_-(l+1)(2l+3)}\left[\frac{1}{2}(l+3)r^2\vec{\nabla}p_l^- - l\vec{r}p_l^-\right]. \tag{27}$$

The pressure of the fluid inside the sphere $p^-=\Sigma_l p_l^-$, so we can see that the final term in this equation is the particular solution to Eq. (15), while the first two terms are the homogeneous solution. The *harmonic functions* q_l^-, w_l^-, and p_l^- satisfy Laplace's equation, $\vec{\nabla}^2\Phi_l^-(r,\theta,\phi)=0$ and must remain finite at the origin $r=0$,

$$\Phi_l^-(r,\theta,\phi) = \sum_{n=-l}^{l} \Phi_{l,n}^- r^l Y_{l,n}(\theta,\phi). \tag{28}$$

An arbitrary harmonic function $\Phi^-(r,\theta,\phi)$ inside the sphere can be written as a linear combination of the functions $\Phi_l^-(r,\theta,\phi)$.

The second part of the solution to the 3D Stokes equation (15) in spherical coordinates $\vec{v}^+$ decays to zero as $r\to\infty$, and thus is suitable for the fluid velocity outside of the membrane given the boundary condition at infinity. This solution can be written as $\vec{v}^+ = \Sigma_{l=1}^{\infty} \vec{v}_l^+$, where the velocity field $\vec{v}_l^+$ is given by Eq. (27) with the replacements $l\to -l-1$ and $\eta_-\to\eta_+$ in the coefficients of Eq. (27). Similarly, any harmonic function $\Phi_l^+(r,\theta,\phi)$ outside the sphere is given by Eq. (28) with the replacement $r^l \to r^{-l-1}$.

In order to enforce the boundary conditions on the surface of the membrane, which have been written in covariant form (see Sec. III), it is convenient to write the bulk fluid velocity components Eq. (27) in covariant form as well,

$$\vec{v}_{l,r}^-(r,\theta,\phi) = \frac{l}{r} w_l^- + \frac{lr}{2\eta_-(2l+3)} p_l^-, \tag{29}$$

$$v_{l,\alpha}^-(r,\theta,\phi) = rR\epsilon_{\alpha\beta} D^\beta q_l^- + D_\alpha w_l^- + \frac{l+3}{2\eta_-(l+1)(2l+3)} r^2 D_\alpha p_l^-. \tag{30}$$

In these equations, the asymmetric tensor $\epsilon_{\alpha\beta}$ and the covariant derivative D_α are defined *on the sphere*. That is, all radial distances in these quantities are set equal to the sphere radius R. Again, we simply make the substitutions $l\to -l-1$, $\eta_-\to\eta_+$ in the coefficients for the covariant velocity components $\vec{v}_{l,r}^+$ and $\vec{v}_{l,\alpha}^+$ outside of the sphere.

C. Point-force response of the combined membrane/embedding fluids system

The membrane is coupled to the embedding fluids via the stick boundary conditions Eqs. (17) and (18) and the stress-balance condition Eq. (21) on the surface of the sphere. Using the normal coordinates for the sphere, given by $(u^1,u^2,u^3)=(\theta,\phi,r-R)$, along with Eqs. (24) and (26), the stick boundary conditions can be written as

$$v_r^\pm(R,\theta,\phi) = 0, \quad D^\alpha v_\alpha^\pm(R,\theta,\phi) = 0, \tag{31}$$

$$\epsilon^{\alpha\gamma} D_\gamma v_\alpha^\pm(R,\theta,\phi) = -\sum_{l,n} \frac{l(l+1)}{R^2} A_{l,n} Y_{l,n}(\theta,\phi). \tag{32}$$

From Eqs. (29) and (30), we see that Eq. (31) causes $w_l^\pm = p_l^\pm = 0$. This implies that shear flows in a spherical membrane do not alter the pressures in the embedding fluids, $p^\pm(r,\theta,\phi)=0$. This is also the case for flat membranes [13].

If we denote the covariant components of the fluid velocity at *all points in space* as $v_i(r,\theta,\phi)$,

$$v_i(r,\theta,\phi) = \begin{cases} v_i^-(r,\theta,\phi) & r<R \\ v_i(\theta,\phi) & r=R \\ v_i^+(r,\theta,\phi) & r>R \end{cases}, \tag{33}$$

then we can show using Eq. (32) that

$$v_i(r,\theta,\phi) = \delta_{\alpha i}^\perp \sum_{l,n} g_l(r) A_{l,n} \epsilon_{\alpha\beta} D^\beta Y_{l,n}(\theta,\phi), \tag{34}$$

where $\delta_{\alpha i}^\perp$ is the in-plane projection operator and

$$g_l(r) = \begin{cases} \left(\frac{r}{R}\right)^{l+1} & r<R \\ \left(\frac{R}{r}\right)^{l} & r>R \end{cases}. \tag{35}$$

We now turn to the stress balance condition. Using Eqs. (20) and (34), we can compute the stresses acting on the membrane due to the embedding fluids inside (−) and outside (+) the spherical membrane. The stress due to the interior fluid is given by $\sigma_{\alpha r}^-$,

$$\sigma_{\alpha r}^-|_{u^3=0} = \frac{\eta_-}{R} \sum_{l,n} (l-1) A_{l,n} \epsilon_{\alpha\beta} D^\beta Y_{l,n}(\theta,\phi). \tag{36}$$

The stress due to the exterior fluid $\sigma_{\alpha r}^+|_{u^3=0}$ can be found using the same substitution pattern given above, which causes $\eta_-(l-1)\to -\eta_+(l+2)$ in this equation.

Using Eqs. (24) and (36), the stress boundary condition Eq. (21) becomes

$$\epsilon^{\alpha\gamma} D_\gamma \sigma_\alpha^{\text{ext}} = \frac{\eta_m}{R^4} \sum_{l,n} l(l+1) s_l A_{l,n} Y_{l,n}(\theta,\phi), \tag{37}$$

where

$$s_l = l(l+1) - 2 + \frac{R}{\ell_-}(l-1) + \frac{R}{\ell_+}(l+2). \tag{38}$$

We have defined two Saffman-Delbrück lengths $\ell_\pm \equiv \eta_m/\eta_\pm$ for each embedding fluid in a manner analogous to the original SD length $\ell_0 \equiv \eta/(\eta_+ + \eta_-)$ introduced for the case of a flat membrane [12].

It now remains only to add the external force applied to the particle in the membrane to generate flows in the membrane (and in the embedding fluids). Using the completeness of the spherical harmonics, this external stress can be written as

$$\sigma_\alpha^{\text{ext}} = \frac{F_{0,\alpha}}{R^2} \sum_{l=0}^{\infty} \sum_{n=-l}^{l} Y_{l,n}(\theta,\phi) Y_{l,n}^*(\theta_0,\phi_0). \tag{39}$$

Solving for the unknown coefficients $A_{l,n}$ in Eq. (37) using the orthonormality of the spherical harmonics completes our solution. We find

$$A_{l,n} = \frac{R^2}{\eta_m s_l l(l+1)} [\epsilon^{\alpha\gamma} F_{0,\alpha} D_\gamma Y_{l,n}^*(\theta,\phi)|_{(\theta_0,\phi_0)}. \tag{40}$$

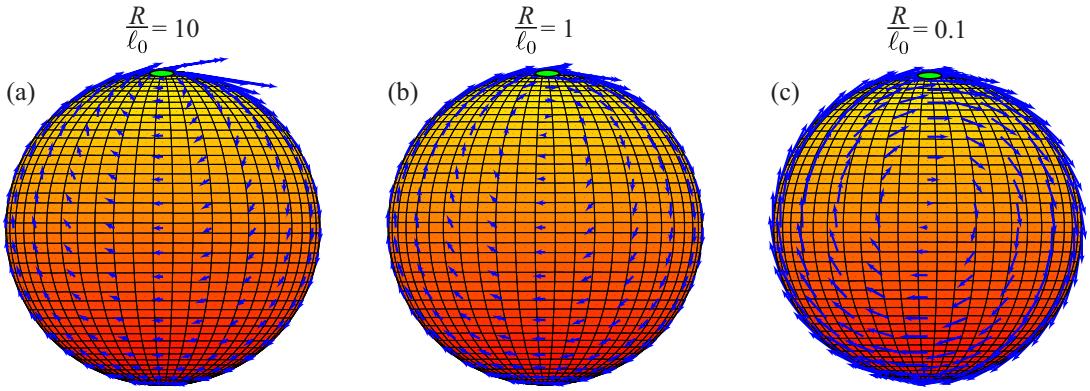

FIG. 1. (Color online) Membrane fluid velocity for a spherical membrane immersed in a symmetric embedding fluid environment ($\eta_+ = \eta_-$) due to a force $\vec{F}_0 = F_{\rm np}\hat{y}$ at the north pole, for decreasing values of R/ℓ_0. The magnitudes of the velocity vectors in each plot are scaled by following scale factors: (a) 15; (b) 2; and (c) $\frac{1}{2}$.

Using the fact that the covariant derivative of a scalar function is identical to a partial derivative, $D_\alpha f = \partial_\alpha f$, it is straightforward to show from Eqs. (34) and (40) that the *physical vector* components of the fluid velocity at the point (θ,ϕ) due to the force applied at the point (θ_0,ϕ_0) are given by $\vec{v}(r,\theta,\phi)\cdot\hat{r}=0$ and

$$\vec{v}(r,\theta,\phi)\cdot\hat{\theta} = \sum_{l=1}^{\infty} \frac{(2l+1)g_l(r)}{4\pi\eta_{\rm m} s_l l(l+1)}[(\vec{F}_0\cdot\hat{\theta}_0)\csc\,\theta\csc\,\theta_0\partial_\phi\partial_{\phi_0}P_l(\cos\,\psi) - (\vec{F}_0\cdot\hat{\phi}_0)\csc\,\theta\partial_\phi\partial_{\theta_0}P_l(\cos\,\psi)], \tag{41}$$

$$\vec{v}(r,\theta,\phi)\cdot\hat{\phi} = \sum_{l=1}^{\infty} \frac{(2l+1)g_l(r)}{4\pi\eta_{\rm m} s_l l(l+1)}[-(\vec{F}_0\cdot\hat{\theta}_0)\csc\,\theta_0\partial_\theta\partial_{\phi_0}P_l(\cos\,\psi) + (\vec{F}_0\cdot\hat{\phi}_0)\partial_\theta\partial_{\theta_0}P_l(\cos\,\psi)]. \tag{42}$$

The Legendre functions $P_l(x)$ arise from using the addition theorem for spherical harmonics to perform the sums over n in Eq. (34). Finally, ψ is the angle between the points (θ,ϕ) and (θ_0,ϕ_0).

For a single point force acting on the membrane, we can place the point force at the north pole and choose $\vec{F}_0 = F_{\rm np}\hat{y}$ without loss of generality. Then, Eqs. (41) and (42) become

$$\vec{v}_{\rm np}(r,\theta,\phi) = -F_{\rm np}\{\sin\,\phi\,\csc\,\theta S_1^+(r,\cos\,\theta)\hat{\theta} + \cos\,\phi[\cot\,\theta S_1^+(r,\cos\,\theta) + S_2^+(r,\cos\,\theta)]\hat{\phi}\}, \tag{43}$$

where the sums $S_n^{\pm}(r,x)$ are defined as

$$S_n^{\pm}(r,x) \equiv \frac{1}{4\pi\eta_{\rm m}}\sum_{l=1}^{\infty}\frac{2l+1}{l(l+1)}\frac{(\pm 1)^{l+1}}{s_l}g_l(r)P_l^n(x). \tag{44}$$

Figure 1 shows the fluid velocity field on a membrane immersed in a symmetric embedding fluid environment (i.e., $\eta_+ = \eta_-$) in response to a point force for a varying values of the dimensionless ratio R/ℓ_0. In each case, we can see a single vortex in the fluid velocity along the line of longitude perpendicular to the force at the north pole; an identical vortex is placed symmetrically on the back side of the sphere (not shown). These two vortices in the membrane fluid velocity are required by the topological constraints placed on all vector fields on a sphere [20]. For large spheres, the vortices sit near the north pole, and the fluid velocity is vanishingly small far from the north pole (for clarity, we have scaled the magnitude of the vectors in Fig. 1 to ensure that the vectors are visible). As we will show below, a particle at the north pole subject to such a force would move through the membrane with a mobility close to that of the corresponding flat membrane. As the radius of the sphere decreases, the magnitude of the membrane fluid velocity increases dramatically, and the vortices migrate to the equator. In this limit, Fig. 1(c) shows that the membrane fluid velocity field approaches that of the uniform rotational motion of a rigid sphere. Indeed, we can show from Eq. (43) that the interior fluid and membrane rotate together as a rigid object when the membrane radius is small. From Eq. (38),

$$\frac{s_1^{-1}}{s_l^{-1}} \sim \frac{\ell_+}{R}l^2 + l\left(\frac{\ell_+}{\ell_-}+1\right) \quad \text{for } l>1. \tag{45}$$

When $R/\ell_+ \ll 1$, this ratio is large and the $l=1$ term will dominate the sums in Eq. (43) as long as ℓ_-/ℓ_+ is not very small. Then, the velocity of the membrane and interior fluid are approximately given by

$$\lim_{R/\ell_+\to 0} \vec{v}_{\rm np}(r,\theta,\phi) = \frac{F_{\rm np}(\hat{x}\times\vec{r})}{8\pi\eta_+ R^2}, \quad \text{for } r \le R. \tag{46}$$

This is precisely the velocity of a rigid sphere rotating about the $\hat{x}$ axis. Thus, in the limit $R/\ell_+ \ll 1$, the applied point force causes the entire sphere to rotate, rather than dragging the particle through the membrane. Because of the high curvature of the membrane, the energy needed to establish the velocity gradients required to move the particle within the membrane becomes prohibitively large. As a result, the force on the north pole causes the entire membrane to rotate rigidly, which dissipates much less energy.

D. Particle mobility

As defined in Sec. III, the particle mobility follows from the membrane velocity at the location of the particle. From Eq. (43), we find [38]

$$\lim_{\theta\to 0} \vec{v}_{\rm np}(\theta,\phi) = F_{\rm np}\hat{y}\sum_{l=1}^{l_{\rm max}} \frac{(2l+1)}{8\pi\eta_{\rm m} s_l} \equiv F_{\rm np}\hat{y}\sum_{l=1}^{l_{\rm max}} S_l. \tag{47}$$

As required by the structure of the two-dimensional Green's function discussed above, the summand in Eq. (47) $\sim 1/l$ for $l \gg 1$, so the sum possesses a short-distance logarithmic divergence that is cut off by the particle size a. This introduces a high-wave-number cutoff $l_{\rm max} \sim 1/a$ to the sum in Eq. (47); we will determine the precise value of $l_{\rm max}$ below.

We have seen that a force on an isolated spherical membrane can give rise to a rigid rotation of the membrane when the radius R is small. This result indicates that the definition of the particle's mobility in the spherical membrane is ambiguous. In response to an applied point force, the membrane picks up a rigid body rotation. Clearly the particle's motion due to this global rotation should not contribute to the definition of its mobility, which concerns the motion of the particle *within* the fluid membrane. However, there are multiple ways to remove that rotation, and each choice generates a slightly different definition of the particle mobility. This issue does not arise for the infinite flat membrane because the membrane velocity field decays sufficiently rapidly at long distance, so that one may conclude that the membrane remains globally at rest. We expect the ambiguity discussed here in terms of the spherical membrane to apply to any compact membrane that has a finite area. To better illustrate the range of choices for the particulate mobility, we discuss three different choices below. For the free mobility, we allow the membrane's global rotation and include the contribution of this motion in the particle's mobility. A more reasonable definition may be found by considering the particle's mobility in a *pinned* membrane, where a constraint force is applied at the antipode of the particle (i.e., south pole) and sets the membrane velocity to zero there. This definition is appropriate for studying particle mobilities on a sphere (e.g., a giant unilamellar vesicle or fluid droplet) that rests on a support such as a glass coverslip. Finally, one may define a mobility in which the particle's velocity is computed in the reference frame that is *co-rotating* with the rigid body motion of the spherical membrane. This amounts to simply subtracting off the $\ell=1$ contribution to the sum in the particle's velocity.

The *free* mobility is defined by the equation

$$\lim_{\theta\to 0} \vec{v}_{\rm np}(\theta,\phi) = \mu_{\rm free}\vec{F}_{\rm np}, \quad \Rightarrow \mu_{\rm free} = \sum_{l=1}^{l_{\rm max}} \frac{(2l+1)}{8\pi\eta_{\rm m} s_l}. \tag{48}$$

The final equality follows from Eq. (47). This result depends on the unknown cutoff parameter $l_{\rm max}$. To determine a value for $l_{\rm max}$, we insist that the mobility of a small particle ($a \ll \ell_0$) in a spherical membrane reduces to that of a flat membrane in the limit of an arbitrarily large sphere, $R\to\infty$. The mobility of a such a particle embedded in a flat membrane is given by [12,13]

$$\mu_{\rm flat} = \frac{1}{4\pi\eta_{\rm m}}\left[\ln\left(\frac{2\ell_0}{a}\right) - \Gamma\right], \tag{49}$$

where Γ is Euler's constant. To obtain the flat-space limit of Eq. (48) we define a wave number $q \equiv l/R$ and convert the sum to an integral. Performing the integral we obtain

$$\lim_{R\to\infty} \mu_{\rm free} = \ln\left[1 + \frac{l_{\rm max}\ell_0}{R}\right], \tag{50}$$

from which we set

$$l_{\rm max} = \frac{2R}{a}e^{-\Gamma}, \tag{51}$$

so that Eq. (50) is consistent with Eq. (49) to leading order in ℓ_0/a.

In the opposite limit of a small spherical membrane, $R/\ell_+ \ll 1$, the $l=1$ term in the mobility Eq. (48) dominates. In this limit, we still take a to be the smallest length in the problem, so $l_{\rm max} \sim R/a$ is still very large and we cannot simply discard the $l \neq 1$ terms in $\mu_{\rm free}$. For these terms, we approximate $s_l \approx l(l+1)-2$; to leading order in $l_{\rm max}$, we find

$$\lim_{R/\ell_+\to 0} \mu_{\rm free} = \frac{1}{8\pi\eta_+ R} + \frac{1}{4\pi\eta_{\rm m}}\left[\ln\left(\frac{2R}{a}\right) - \frac{11}{12}\right]. \tag{52}$$

The first term is the $l=1$ term, which is given precisely by the rotational mobility of a solid sphere, as expected; the second term arises from the $l \neq 1$ terms. The dominance of the $l=1$ term in the sum demonstrates that the particle's mobility mainly reflects the rigid body rotation of the sphere, plus logarithmic corrections.

One way to eliminate the rigid rotation of the sphere is to introduce a pinning force on the membrane that prevents such a motion. In order to minimize the effect of this pinning force on the nonrotational contributions to the particle mobility, we place the pinning force at the south pole of the membrane. The pinning force acts as a constraint fixing the membrane velocity to be zero at the south pole. The calculation of the membrane velocity field in response to the combination of the applied force at the north pole (i.e., the particle) and the constraint (pinning) force at the south pole presents no new difficulties. Due to the linearity of the equations in velocity, the effects of the two forces simply add. In addition to preventing the rotation of the membrane, this pinning force approximates the configuration of the experiments in Ref. [8]. The rigid rotation of the sphere due to a

force in the $+\hat{y}$ direction at the north pole generates a velocity in the $-\hat{y}$ direction at the south pole, so the pinning force must point in the $+\hat{y}$ direction. These two forces produce oppositely directed torques about the center of the sphere, but seemingly act in concert to translate it in the $+\hat{y}$ direction. However, this translational motion is prevented by our choice of boundary conditions. Using Eqs. (41) and (42), we find that the velocity $\vec{v}_{\rm sp}$ due to the force at the south pole is

$$\vec{v}_{\rm sp}(r,\theta,\phi) = F_{\rm sp} \sin\phi \csc\theta S_1^-(r,\cos\theta)\hat{\theta} + F_{\rm sp}\cos\phi[\cot\theta S_1^-(r,\cos\theta) + S_2^-(r,\cos\theta)]\hat{\phi}, \tag{53}$$

Using linear superposition, the total velocity for the pinned membrane is

$$\vec{v}_{\rm pin}(r,\theta,\phi) = \vec{v}_{\rm np}(r,\theta,\phi) + \vec{v}_{\rm sp}(r,\theta,\phi). \tag{54}$$

The magnitude of the pinning force $F_{\rm sp}$ is set by the constraint that the membrane velocity vanish at the south pole. We find that the pinning force at the south pole is proportional to the applied force on the particle, $F_{\rm sp} = \frac{S_{\rm pin}}{\mu_{\rm free}} F_{\rm np}$, where

$$S_{\rm pin} \equiv \sum_{l=1}^{l_{\rm max}} \frac{(-1)^{l+1}(2l+1)}{8\pi\eta_{\rm m} s_l}. \tag{55}$$

Then, the mobility $\mu_{\rm pin}$ of the particle at the north pole of a pinned spherical membrane is given by

$$\mu_{\rm pin} = \mu_{\rm free}\left[1 - \left(\frac{S_{\rm pin}}{\mu_{\rm free}}\right)^2\right]. \tag{56}$$

As one might expect, $\mu_{\rm pin} < \mu_{\rm free}$ generally. In addition, in the flat-membrane limit, $R \to \infty$, the correction to $\mu_{\rm pin}$ due to the rigid rotation of the sphere vanishes, so that $\mu_{\rm pin} \approx \mu_{\rm free} \to \mu_{\rm flat}$. More interestingly, in the limit of small spheres, $R/\ell_+ \ll 1$, the rigid rotation term that dominates the free mobility result is absent from $\mu_{\rm pin}$. To determine the asymptotic behavior of $\mu_{\rm pin}$ in this limit, we use Eq. (52) and approximate $s_l \approx l(l+1)-2$ in $S_{\rm pin}$, as we did for $\mu_{\rm free}$. To $\mathcal{O}[(\frac{R}{a})^0]$,

$$\lim_{R/\ell_+ \to 0} \mu_{\rm pin} = \frac{1}{2\pi\eta_{\rm m}}\left[\ln\left(\frac{2R}{a}\right) - \frac{1}{2}\right]. \tag{57}$$

The pinned membrane mobility is perhaps most relevant to the commonly encountered experimental system of a supported droplet, but it also appears to be a somewhat arbitrary definition and has the disadvantage that the mobility of a particle on a ostensively uniform membrane becomes a function of position. We have considered only the case in which the pinning is applied antipodally; a spectrum of mobility results can be obtained by changing the separation between the particle and the pinning site. To eliminate this effect, we can define a *co-rotating* mobility in which we subtract the rigid body rotation by determining the resultant particle velocity in a frame co-rotating with the rigid body motion of the membrane. This amounts to simply dropping the term in the mobility that corresponds to the rigid rotation of the sphere, i.e., the $l=1$ term. Then, we find

$$\mu_{\rm corot} = \sum_{l=2}^{l_{\rm max}} \frac{2l+1}{8\pi\eta_{\rm m} s_l}. \tag{58}$$

Once again, in the flat-space limit $R \to \infty$, $\mu_{\rm corot} \approx \mu_{\rm free} \to \mu_{\rm flat}$. The small sphere ($R/\ell_+ \ll 1$) behavior of $\mu_{\rm corot}$ follows directly from Eq. (52):

$$\lim_{R/\ell_+ \to 0} \mu_{\rm corot} = \frac{1}{4\pi\eta_{\rm m}}\left[\ln\left(\frac{2R}{a}\right) - \frac{11}{12}\right]. \tag{59}$$

For both of these particle mobilities, we can see that for highly curved membranes $R/\ell_+ \ll 1$, the long-distance cutoff to the logarithmic divergence in the mobility is the membrane radius R, rather than the Saffman-Delbrück length ℓ_0 that appears in the flat membrane mobility Eq. (49) [19]. We expect that particle mobilities are generically suppressed by curvature whenever the radius of curvature becomes smaller than the SD length. Although the appearance of R as the long-distance cutoff is generically expected, the prefactor clearly depends on the definition of mobility used, or equivalently the way in which the mobility is experimentally measured.

In Figs. 2(a)–2(c), we plot the free mobility $\mu_{\rm free}$, the mobility in a pinned membrane $\mu_{\rm pin}$, and the co-rotating mobility $\mu_{\rm corot}$, respectively, as a function of the ratio R/ℓ_+ for a variety of internal viscosities (i.e., values of ℓ_-; see caption). All of the mobilities approach their flat-space limits when $R/\ell_+ \gg 1$. They also approach the expected asymptotic results in the limit $R/\ell_+ \ll 1$, Eqs. (52), (57), and (59) for Figs. 2(a)–2(c), respectively.

At intermediate curvatures, we can see that the asymmetry between the interior and exterior fluid viscosities influences the behavior of the particle mobility as it approaches the flat-space limit. When the more viscous fluid is bounded by the spherical membrane, i.e., $\eta_+/\eta_- > 1$ [green (gray) curves], it dissipates less energy than in the flat case, where it is unbounded. As a result, the mobility in the spherical membrane is larger than in the flat membrane, so the approach to the flat-space limit is from above. Conversely, when $\eta_+/\eta_- < 1$ (dotted curves), the mobility is suppressed relative to that of the flat membrane. We note that the behavior of $\mu_{\rm pin}$ is markedly different that of $\mu_{\rm corot}$ at intermediate curvatures. In particular, $\mu_{\rm pin}$ has a strongly nonmonotonic behavior at intermediate curvatures, whereas $\mu_{\rm corot}$ is essentially always a monotonically decreasing function of R/ℓ_+, only displaying a weak nonmonotonic behavior for $\eta_+ > \eta_-$ (due to the asymmetry effect described above). This difference is caused by the different ways in which the effect of the membrane's rigid rotation is removed from these mobilities. For $\mu_{\rm corot}$, the rotational motion is excluded from the mobility for all membrane curvatures, whereas for $\mu_{\rm pin}$ this motion is only completely removed for membranes with high curvatures. As a result, the rotational motion—which leads to an increase in the mobility as R decreases [see Fig. 2(a)]—does contribute to $\mu_{\rm pin}$ for intermediate curvatures, causing it to increase as R decreases for intermediate values of R/ℓ_+, as seen in Fig. 2(b).

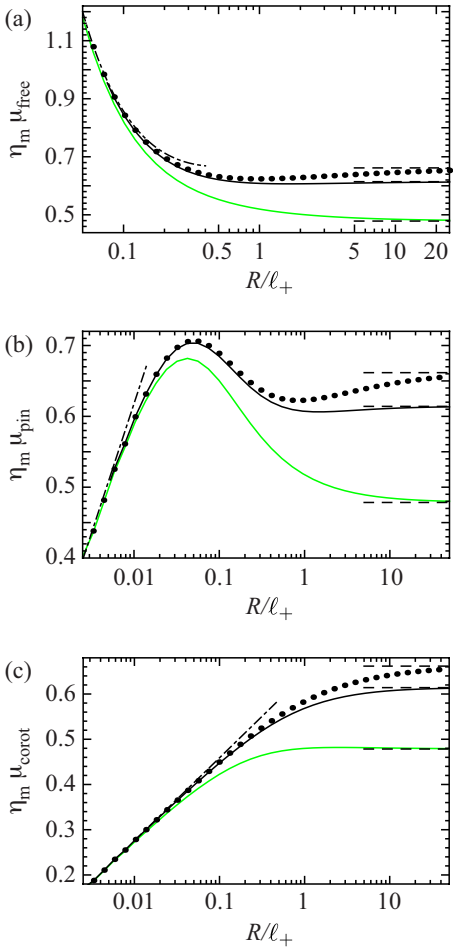

FIG. 2. (Color online) Dimensionless mobilities of a pointlike particle embedded in a sphere as a function of the ratio R/ℓ_+ for $\ell_+/a=10^3$ and $\ell_-=0.1\ell_+$ [green (gray) curves], $\ell_-=\ell_+$ (black curves), and $\ell_-=10\ell_+$ (dotted curves). The dot-dashed curves are the appropriate analytic expressions for the mobilities in the limit $R/\ell_+\to 0$ (see text); the dashed curves are the flat-space limits, Eq. (49). (a) "Free" mobility μ_{free}; (b) mobility in a pinned membrane μ_{pin}; and (c) mobility in the co-rotating frame of reference, μ_{corot}.

V. CYLINDRICAL MEMBRANE

In this section, we turn to the case of a cylindrical membrane of radius R. The organization of this section follows that of the previous one. First, we find the shear modes of the membrane. We then give the solution to the Stokes equation for the embedding fluids inside and outside the cylinder. Using these results, we determine the response of the membrane/embedding fluids system to an in-plane point force in the membrane and investigate the membrane flows and the particle mobility in detail.

A. Membrane modes

For a cylinder of radius R, the Gaussian curvature vanishes, $K=0$. Equation (8) then states that the covariant derivatives commute. In fact they are equal to the usual partial derivatives, $D_\alpha=\partial_\alpha$. Choosing $\hat{z}$ to be parallel to the cylinder axis, the eigenfunctions of the Laplacian are simply the Fourier modes $e^{in\theta+iqz}$. The periodicity of the angular variable requires that n be restricted to the integers. From Eq. (14), the eigenfunctions and eigenvalues for the shear modes of the cylinder are

$$\Phi(\vec{x};\Lambda)=\exp[e^{i\Lambda_\mu x^\mu}],\quad \lambda(\Lambda)=-\eta_m\Lambda_\alpha\Lambda^\alpha, \tag{60}$$

where the covariant vector Λ_α is defined as

$$\Lambda_\theta=n,\quad \Lambda_z=q,\quad \Rightarrow \Lambda_\alpha\Lambda^\alpha=\left[q^2+\frac{n^2}{R^2}\right] \tag{61}$$

The general membrane velocity field Eq. (12) is thus

$$v_\alpha(\theta,z)=i\epsilon_{\alpha\beta}\int d\Lambda A(\Lambda)\Lambda^\beta e^{i\Lambda_\mu x^\mu}, \tag{62}$$

where

$$\int d\Lambda \equiv \sum_{n=-\infty}^{\infty}\int_{-\infty}^{\infty} dq. \tag{63}$$

B. Solution to the 3D Stokes equation

The solution to the Stokes equation (15) in cylindrical coordinates can be written as [35]

$$\vec{v}^{\pm}(r,\theta,z)=\vec{\nabla}f^{\pm}(r,\theta,z)+\vec{\nabla}\times[g(r,\theta,z)\hat{z}] + r\partial_r[\vec{\nabla}h^{\pm}(r,\theta,z)]+\partial_z h^{\pm}(r,\theta,z)\hat{z}, \tag{64}$$

$$p^{\pm}(r,\theta,z)=-2\eta_{\pm}\partial_z^2 h^{\pm}(r,\theta,z), \tag{65}$$

where $f^{\pm}(r,\theta,z)$, $g^{\pm}(r,\theta,z)$, and $h^{\pm}(r,\theta,z)$ are harmonic functions in cylindrical coordinates. Motivated by the form of the membrane velocity Eq. (62), we write a harmonic function $\Psi(r,\theta,z)$ in cylindrical coordinates as

$$\Psi(r,\theta,z)=e^{i\Lambda_\mu x^\mu}\psi(r). \tag{66}$$

Then, it is straightforward to show that Laplace's equation $\vec{\nabla}^2\Psi=0$ becomes the modified Bessel's equation for $\psi(r)$, whose homogeneous solutions are the modified Bessel functions of the first and second kind, $K_n(qr)$ and $I_n(qr)$, respectively. Since $\lim_{x\to 0}K_n(x)=\lim_{x\to\infty}I_n(x)=\infty$, the functions $K_n(qr)$ are the appropriate solutions for the exterior embedding fluid, while the functions $I_n(qr)$ are the appropriate solutions for the interior one. Thus, we can write

$$\Psi^{\pm}(r,\theta,z)=\int d\Lambda e^{i\Lambda_\mu x^\mu}\Psi^{\pm}(\Lambda)\xi_n^{\pm}(qr), \tag{67}$$

where

$$\xi_n^{+}(qr)\equiv K_n(|q|r),\quad \xi_n^{-}(qr)\equiv I_n(|q|r). \tag{68}$$

Here, the absolute values are needed to ensure the reality of the harmonic functions.

As in the case of spherical membranes, the boundary conditions at the membrane surface are most easily enforced using covariant notation. If we write the covariant velocity components as

$$v_i^{\pm}(r,\theta,z) = \int d\Lambda e^{i\Lambda_\mu x^\mu} w_i^{\pm}(\Lambda,r), \tag{69}$$

then using Eq. (64),

$$w_r^{\pm}(\Lambda,r) = |q|\tilde{\xi}_n^{\pm}(qr)F^{\pm}(\Lambda) + \frac{in}{r}\xi_n^{\pm}(qr)G^{\pm}(\Lambda) + H^{\pm}(\Lambda)\left[-|q|\tilde{\xi}_n^{\pm}(qr) + r\left(q^2 + \frac{n^2}{r^2}\right)\xi_n^{\pm}(qr)\right], \tag{70}$$

$$w_\theta^{\pm}(\Lambda,r) = im\xi_n^{\pm}(qr)F^{\pm}(\Lambda) - |q|r\tilde{\xi}_n^{\pm}(qr)G^{\pm}(\Lambda) + inH^{\pm}(\Lambda)[|q|r\tilde{\xi}_n^{\pm}(qr) - \xi_n^{\pm}(qr)], \tag{71}$$

$$w_z^{\pm}(\Lambda,r) = iq\xi_n^{\pm}(qr)F^{\pm}(\Lambda) + iqH^{\pm}(\Lambda)[|q|r\tilde{\xi}_n^{\pm}(qr) + \xi_n^{\pm}(qr)]. \tag{72}$$

Here, $F^{\pm}(\Lambda)$, $G^{\pm}(\Lambda)$, and $H^{\pm}(\Lambda)$ are the coefficients of the harmonic functions $f^{\pm}(r,\theta,z)$, $g^{\pm}(r,\theta,z)$, and $h^{\pm}(r,\theta,z)$, respectively [see Eq. (67)], and

$$\tilde{\xi}^{+}(qr) \equiv \left.\frac{dK_n(u)}{du}\right|_{u=|q|r}, \quad \tilde{\xi}^{-}(qr) \equiv \left.\frac{dI_n(u)}{du}\right|_{u=|q|r}. \tag{73}$$

C. Point-force response of the combined membrane/embedding fluids system

We now couple the membrane flows to the flows in the embedding fluids using the stick boundary conditions, Eqs. (17) and (18), and the stress-balance condition Eq. (21). We begin with the stick boundary conditions. Using Eq. (69), Eqs. (17) and (18) become, respectively,

$$w_r^{\pm}(\Lambda,R) = 0, \quad \Lambda^\alpha w_\alpha^{\pm}(\Lambda,R) = 0, \tag{74}$$

$$i\epsilon^{\alpha\gamma}\Lambda_\gamma w_\alpha^{\pm}(\Lambda,R) = -\Lambda_\beta\Lambda^\beta A(\Lambda). \tag{75}$$

Applying Eqs. (70)–(72), these boundary conditions become a system of six linear equations relating the coefficients $F^{\pm}$, $G^{\pm}$, and $H^{\pm}$ to the membrane shear mode amplitudes A. In the case of a spherical membrane, the rotational symmetry between the in-plane coordinates θ and ϕ and the simple power-law dependence of the harmonic functions Eq. (28) on the out-of-plane coordinate r greatly simplified the solution of the analogous boundary conditions. For the cylinder, the solutions of Eqs. (74) and (75), although straightforward to obtain, are complex and unilluminating; we forgo writing these expressions here.

Using Eqs. (70)–(72), we can compute the terms in the stress-balance condition Eq. (21) due to the flows in the embedding fluids in terms of the coefficients $F^{\pm}$, $G^{\pm}$, and $H^{\pm}$. From the stick boundary conditions Eqs. (74) and (75), we find after some algebra that

$$\epsilon^{\alpha\gamma}D_\gamma\sigma_{\alpha r}^{\pm}|_{r=R} = -\eta_{\pm}\int D\Lambda e^{i\Lambda_\mu x^\mu}\frac{A(\Lambda)}{R^3}C^{\pm}(\Lambda), \tag{76}$$

with

$$C^{\pm}(\Lambda) = C_n^{\pm}(k) = \frac{2n^2[\rho^{\pm}(\Lambda)]^3 + (n^2+k^2)^2[\rho^{\pm}(\Lambda)]^2 + 2\rho^{\pm}(\Lambda)(k^4-n^4) - (k^2+n^2)^3}{\rho^{\pm}(\Lambda)k^2 - [\rho^{\pm}(\Lambda)-n][\rho^{\pm}(\Lambda)+n][\rho^{\pm}(\Lambda)+2]}, \tag{77}$$

and where we have defined

$$k \equiv qR. \quad \rho^{\pm}(\Lambda) \equiv \frac{|k|\tilde{\xi}_n^{\pm}(k)}{\xi_n^{\pm}(k)}. \tag{78}$$

The stress due to the externally applied in-plane point force $\vec{F}_0$ acting at the point (θ_0, z_0) in the membrane can be written as

$$\sigma_\alpha^{\text{ext}} = \frac{F_{0,\alpha}}{4\pi^2 R}\int D\Lambda \exp[i\Lambda_\mu x^\mu - i(n\theta_0 + qz_0)]. \tag{79}$$

From Eqs. (76) and (79), we solve the stress-balance condition Eq. (21) to determine the amplitudes $A(\Lambda)=A_n(k)$ of the membrane shear modes generated by the applied force. We find

$$A_n(k) = -\frac{iR^2 e^{-i(n\theta_0+k\zeta_0)}}{4\pi^2\eta_m c_n(k)}[k(\vec{F}_0\cdot\hat{\theta}_0) - n(\vec{F}_0\cdot\hat{z})], \tag{80}$$

where $\zeta \equiv z/R$ and

$$c_n(k) \equiv (k^2+n^2)^2 + \frac{R}{\ell_+}C_n^{+}(k) - \frac{R}{\ell_-}C_n^{-}(k). \tag{81}$$

From these amplitudes, the membrane velocity field is found to be

$$\vec{v}(\theta,\zeta) = (\vec{F}_0\cdot\hat{\theta}_0)[\chi_1(\Delta\theta,\Delta\zeta)\hat{\theta} - \chi_0(\Delta\theta,\Delta\zeta)\hat{z}] + (\vec{F}_0\cdot\hat{z})[\chi_{-1}(\Delta\theta,\Delta\zeta)\hat{z} - \chi_0(\Delta\theta,\Delta\zeta)\hat{\theta}], \tag{82}$$

where $\Delta\theta=\theta-\theta_0$, $\Delta\zeta=\zeta-\zeta_0$, and

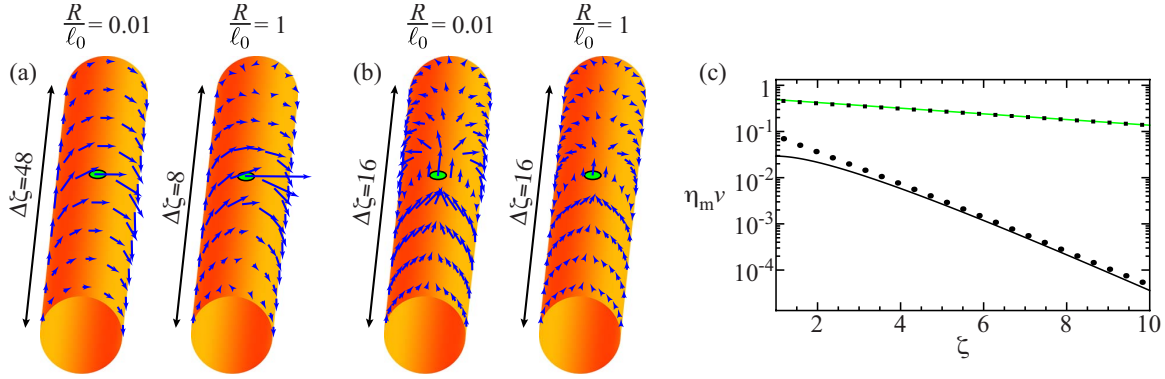

FIG. 3. (Color online) Membrane fluid velocity for a cylindrical membrane immersed in a symmetric external fluid environment ($\eta_+ = \eta_-$) due to a force (a) $\vec{F}_0 = F_0\hat{\theta}_0$ and (b) $\vec{F}_0 = F_0\hat{z}$ at the origin, for $R/\ell_0 = 0.01$ and 1. The magnitudes of the velocity vectors in the plot for $\vec{F}_0 = F_0\hat{\theta}$, $R/\ell_0 = 0.01$ are scaled by a factor of 0.1 relative to the other plots. In addition, the region of the cylinder pictured for each cases is variable; the length of the cylinder is indicated next to each figure. (c) Detail of the velocity magnitudes along the line $\theta = 0$, $\zeta > 0$ for the velocities for $R/\ell_0 = 0.01$. The points are the exact numerical solutions for $\vec{F}_0 = F_0\hat{\theta}_0$ (squares) and $\vec{F}_0 = F_0\hat{z}$ (circles); the solid curves are the analytic expressions, Eq. (85) [green (gray) curve] and Eq. (86) (black curve), respectively.

$$\chi_p(\theta,\zeta) = \frac{1}{4\pi^2\eta_m}\sum_{n=-\infty}^{\infty}\int_{-\infty}^{\infty} dk \frac{k^{1+p}n^{1-p}}{c_n(k)} e^{in\theta+ik\zeta}. \quad (83)$$

Figures 3(a) and 3(b) show the membrane velocity fields on a cylinder in a symmetric fluid environment subject to a force applied at $(\theta_0, z_0) = (0,0)$ in the $\hat{\theta}$ and $\hat{z}$ directions, respectively, at both high and low values of the membrane curvature. For a force in the $\hat{\theta}$ direction, the velocity magnitude increases dramatically as the membrane radius is decreased. For a force in the $\hat{z}$ direction, the effect of curvature is much weaker. This can be seen in the scaling factors chosen for the velocity vectors in Fig. 3: the scaling factor is 10 times larger for $R/\ell_0 = 0.01$ than it is for $R/\ell_0 = 1$ in Fig. 3(a); by contrast, the scales in these two cases in Fig. 3(b) are the same. In addition, we can see in Fig. 3(c) that in the limit $R/\ell_- \ll 1$ the velocity field decays much more slowly away from the particle for a force in the $\hat{\theta}$ direction that it does for a force in the $\hat{z}$ direction.

We have seen in the previous section that a point force on a spherical membrane causes the membrane and interior fluid to rotate rigidly when the curvature is high. Such rigid rotational motion is impossible in response to a point force on an infinite cylinder: for any finite point force, the membrane velocity field must decay sufficiently rapidly at large distances from the point where the force is applied. However, we can show analytically that in the limit $R/\ell_- \ll 1$ a force in the $\hat{\theta}$ direction can cause a flow that *locally* corresponds to a rigid rotation of the cylinder. That is, the membrane velocity becomes roughly independent of the polar angle θ but still decays along the cylinder axis. A force in the $\hat{z}$ direction does not induce such rotational motion for any value of R, so the membrane velocity field always exhibits a strong θ-dependence. The local rigid rotation of the cylinder dissipates much less energy in the membrane and interior fluids, just as the *complete* rigid rotation of the spherical membrane and interior fluid causes *no* dissipation in these fluids. As a result, the magnitude of the membrane velocity induced by a force in the $\hat{\theta}$ direction increases when the cylinder radius is very small, and this velocity decays much more slowly away from the particle than the velocity induced by a force in the $\hat{z}$ direction on the same membrane. This is precisely the behavior seen in Fig. 3.

In the small R limit, we can use the asymptotic behavior of Eq. (81) to determine the membrane velocity. Using the properties of modified Bessel functions, it is straightforward to show that the appropriate definition of the small radius condition for the cylinder is $R/\ell_- \to 0$, and that

$$\lim_{R/\ell_-\to 0} c_n(k) = \begin{cases} k^4 + 2k^2R/\ell_- & n = 0 \\ (k^2+n^2)^2 & n \geq 1 \end{cases}. \quad (84)$$

By contrast, the appropriate definition of the small radius condition for the sphere is $R/\ell_+ \to 0$. This difference reflects that fact that, at high curvature, the fluid inside the sphere rotates rigidly and thus dissipates no energy, whereas for the cylinder energy dissipation by the interior fluid dominates in this limit.

For a force in the $\hat{\theta}$ direction, the $n=0$ term dominates the sum over n in Eq. (82). We can see immediately from Eq. (83) that this term is independent of θ. This is precisely the locally rigid rotational motion described above. For $|z|/R \gg 1$ we find that the velocity field decays exponentially along the cylinder. To leading order in $|z|/R$,

$$\lim_{R/\ell_-\to 0} \vec{v}(\theta,z) \approx \frac{F_\theta\hat{\theta}}{4\pi\eta_m}\sqrt{\frac{\ell_-}{2R}}\exp\left[-\frac{|z|\sqrt{2}}{\sqrt{\ell_- R}}\right], \quad (85)$$

In contrast, for a force along the $\hat{z}$ direction, the $n=0$ terms vanish and the velocity field still displays a strong angular dependence in this limit

$$\lim_{R/\ell_-\to 0} \vec{v}(\theta,z) \approx \frac{F_z e^{-|z|/R}}{4\pi\eta_m R}[|z|\cos\theta\hat{z} + z\sin\theta\hat{\theta}]. \quad (86)$$

We can also see that the decay length L_d for the membrane velocity induced by the force in the $\hat{\theta}$ direction ($L_d = \sqrt{R\ell_-}$) is

much larger than that of the force in the $\hat{z}$ direction ($L_d=R$). These expressions agree very well with the numeric results; see Fig. 3(c).

D. Particle mobility

The cylinder breaks the in-plane rotational symmetry of the membrane, leading to a nontrivial mobility tensor. This tensor can be completely characterized by two scalar quantities: μ_z and μ_θ, the mobilities in response to forces directed along the $\hat{z}$ and $\hat{\theta}$ directions, respectively. The simplest definition of these mobilities follows from the membrane velocity for a "free" membrane, Eq. (82), as is standard in the consideration of mobilities in a flat membrane of infinite extent. These definitions include any contributions from the local rotational motion of the membrane. As discussed above, such a rotation does not occur in response to a force along the $\hat{z}$ direction. As a result, the mobility along the cylinder axis that follows from Eq. (82) is the *only* mobility definition needed for motion in this direction, so we denote this mobility μ_z. For a force in the $\hat{\theta}$ direction, one can introduce alternate definitions of the mobility that eliminate the effect of local rigid rotations in a manner analogous to that discussed for the case of the spherical membrane.

The two independent mobilities for a free cylindrical membrane μ_z and $\mu_{\theta,\text{free}}$ can be found from Eq. (82). In particular, the velocity of a particle in a free cylindrical membrane in response to a force $\vec{F}_0$ is given by

$$\vec{v}(\theta_0,z_0) \equiv (\vec{F}_0\cdot\hat{z})\mu_z\hat{z} + (\vec{F}_0\cdot\hat{\theta}_0)\mu_{\theta,\text{free}}\hat{\theta}, \tag{87}$$

where

$$\mu_z = \frac{1}{4\pi^2\eta_\text{m}}\sum_{n=-N}^{N}\int_{-K}^{K} dk \frac{n^2}{c_n(k)}, \tag{88}$$

$$\mu_{\theta,\text{free}} = \frac{1}{4\pi^2\eta_\text{m}}\sum_{n=-N}^{N}\int_{-K}^{K} dk \frac{k^2}{c_n(k)}. \tag{89}$$

As with the spherical membrane, we choose the cutoffs N and K so as to reproduce the correct flat-space limit of the mobility. In this limit, we define the two-dimensional wave number $\tilde{q}_1 \equiv k/R$, $\tilde{q}_2 \equiv n/R$. The sum on n becomes an integral over $\tilde{q}_2$,

$$\sum_{n=-N}^{N}\int_{-K}^{K} dk \to R^2\int_{-K/R}^{K/R} d\tilde{q}_1\int_{-N/R}^{N/R} d\tilde{q}_2. \tag{90}$$

Using the properties of modified Bessel functions, one can show that

$$\lim_{R\to\infty} c_n(k) = R^4\tilde{q}^3\left[\tilde{q}+\frac{1}{\ell_0}\right]. \tag{91}$$

The two mobilities Eqs. (88) and (89) must become identical in the large R limit, so we must set $K=N$. Then, it is straightforward to show that

$$4\pi\eta_\text{m}\lim_{R\to\infty}\begin{Bmatrix}\mu_z\\ \mu_{\theta,\text{free}}\end{Bmatrix} = \ln\left(2+\frac{2K\ell_0}{R}\right) - \frac{2C}{\pi}, \tag{92}$$

where C is Catalan's constant. If we set $K=\frac{R}{a}\exp(\frac{2C}{\pi}-\Gamma)$, we obtain the necessary agreement with the SD result for the flat membrane, Eq. (49), to leading order in ℓ_0/a.

We now turn to the more interesting limit of high curvature: $R/\ell_-\to 0$. Using Eq. (84) to evaluate the integrals and sums in Eqs. (88) and (89), we find, to $\mathcal{O}[(\frac{R}{a})^0]$,

$$\lim_{R/\ell_-\to 0}\mu_z = \frac{1}{4\pi\eta_\text{m}}\left[\ln\left(\frac{R}{a}\right)+\frac{1}{2}\right], \tag{93}$$

$$\lim_{R/\ell_-\to 0}\mu_{\theta,\text{free}} = \frac{1}{4\pi\eta_\text{m}}\left[\sqrt{\frac{\ell_-}{2R}}+\ln\left(\frac{R}{a}\right)-\frac{1}{2}\right]. \tag{94}$$

In this limit of high curvature, the mobility tensor becomes strongly anisotropic. As expected, the force parallel to the long axis of the cylinder does not cause the membrane to rotate, so the mobility μ_z is logarithmically suppressed as $R/\ell_-\to 0$. By contrast, the mobility is direction perpendicular to this long axis diverges as $R^{-1/2}$. This divergence is much slower than the R^{-1} divergence found in the case of a free spherical membrane because the rotational motion in the cylinder is *local*: dissipative shear stresses are still set up in the interior fluid and in the membrane in this limit, unlike the global rigid rotation seen for the spherical membrane. This also explains why the leading order term in Eq. (94) depends on the membrane and interior fluid viscosities, whereas the leading order term in Eq. (52) is independent of these quantities.

In order to eliminate the contribution of the local rigid rotation of the membrane to the mobility μ_θ, we can use a pinning force to prevent this rotational motion, as we did for the spherical membrane. In particular, we examine the mobility of a particle placed at $(\theta_0,z_0)=(0,0)$ in a membrane pinned on its opposite side, $\theta_\text{pin}=\pi$. One may imagine either that this pinning force acts along the line of contact between the cylinder and a supporting plane or that the pinning force acts only at one point directly below the particle. We choose the latter case here, but the former is equally possible to analyze by considering the effect of a line of regularly spaced pinning forces along the bottom of the cylinder. In the limit that this spacing is small compared to the two SD lengths, this calculation will determine the effect of a pinning contact line. Instead, we apply a single pointlike force $\vec{F}_0 = F_\text{pin}\hat{\theta}_\text{pin} = -F_\text{pin}\hat{y}$ at the point $(\theta_\text{pin},z_\text{pin})=(\pi,0)$. From Eq. (82), we calculate the total velocity field $\vec{v}_\text{pin}$ in response to these two forces,

$$\vec{v}_\text{pin}(\theta,\zeta) = \frac{1}{4\pi^2\eta_\text{m}}\sum_{n=-\infty}^{\infty}\int_{-\infty}^{\infty} dk \frac{e^{in\theta+ik\zeta}}{c_n(k)} \times[F_0-(-1)^nF_\text{pin}][k^2\hat{\theta}-km\hat{z}]. \tag{95}$$

Setting the magnitude F_pin of the pinning force by requiring the total velocity vanish at the point $(\theta_\text{pin},z_\text{pin})$, we find

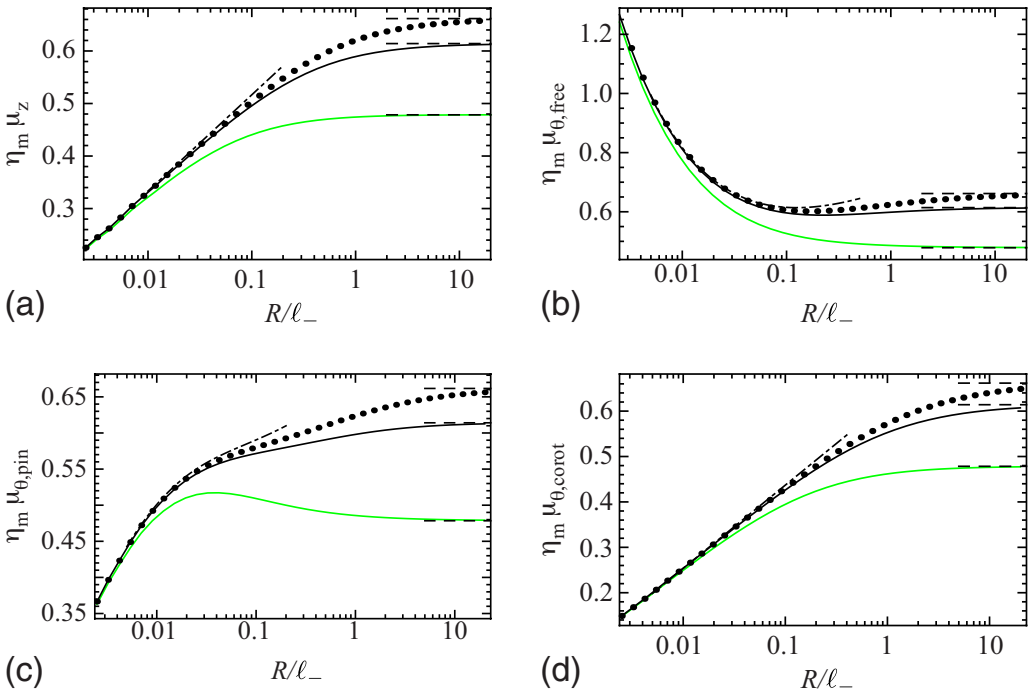

FIG. 4. (Color online) Dimensionless mobilities of a pointlike particle embedded in a cylindrical membrane as a function of the ratio R/ℓ_- for $\ell_-/a=4*10^3$ and $\ell_+=0.1\ell_-$ [green (gray) curves], $\ell_+=\ell_-$ (black curves), and $\ell_+=10\ell_-$ (dotted curves). The dot-dashed curves are the analytic expressions for the mobilities in the limit $R/\ell_+\to 0$ (see text); the dashed curves are the flat-space limits, Eq. (49). (a) Mobility μ_z for a particle subject to a force in the $\hat{z}$ direction. (b), (c), and (d) Mobilities for a particle subject to a force in the $\hat{\theta}$ direction: (b) in a "free" membrane; (c) in a pinned membrane; (d) in a locally co-rotating frame of reference.

$$F_{\mathrm{pin}} = \frac{P}{\mu_{\theta,\mathrm{free}}} F_0, \tag{96}$$

where

$$P \equiv \frac{1}{4\pi^2 \eta_m} \sum_{n=-\infty}^{\infty} \int_{-\infty}^{\infty} \frac{k^2 dk}{c_n(k)}. \tag{97}$$

The particle's mobility in the pinned membrane is

$$\mu_{\theta,\mathrm{pin}} = \mu_{\theta,\mathrm{free}} \left[1 - \left(\frac{P}{\mu_{\theta,\mathrm{free}}} \right)^2 \right]. \tag{98}$$

As with the spherical membrane, the pinning force (i.e., the sum P) vanishes in the flat-space limit $R\to\infty$, and $\mu_{\theta,\mathrm{pin}} \to \mu_{\mathrm{flat}}$. In the limit $R/\ell_-\to 0$, we use Eq. (84) to determine P to $\mathcal{O}[(\frac{R}{a})^0]$,

$$\lim_{R/\ell_-\to 0} P = \frac{1}{4\pi\eta_m} \left[\sqrt{\frac{\ell_-}{2R}} - \ln\left(\frac{R}{a}\right) \right]. \tag{99}$$

Combining this result with the free membrane mobility shown in Eq. (94), we find that the particle's mobility in the pinned membrane can be written as

$$\lim_{R/\ell_-\to 0} \mu_{\theta,\mathrm{pin}} = \frac{1}{2\pi\eta_m} \left[\ln\left(\frac{2R}{a}\right) - \frac{1}{2} \right] * \left\{ 1 - \frac{\ln\left(\frac{2R}{a}\right) - \frac{1}{2}}{\sqrt{\frac{2\ell_-}{R}} + 2\ln\left(\frac{R}{a}\right) - 1} \right\}, \tag{100}$$

Here, the second term in brackets is the next-to-leading-order contribution to the mobility. For the spherical membrane, this term was $\mathcal{O}(R/\ell_+)$ and thus negligible. In this case, however, the next-to-leading-order contribution is much larger—$\mathcal{O}(\sqrt{R/\ell_-})$—and must be kept in order to obtain good agreement with the numerical results.

Again in partial analogy to the case of the spherical membrane, we can define another mobility $\mu_{\theta,\mathrm{corot}}$ in a frame that is co-rotating with the locally defined rigid body motion of the cylinder. This amounts to dropping the $n=0$ from Eq. (89),

$$\mu_{\theta,\mathrm{corot}} = \frac{1}{2\pi^2 \eta_m} \sum_{n=1}^{N} \int_{-K}^{K} dk \frac{k^2}{c_n(k)}. \tag{101}$$

Returning to the flat-space limit $R\to\infty$, the term corresponding to the local rotation becomes insignificant, so $\mu_{\theta,\mathrm{corot}} \to \mu_{\mathrm{flat}}$. In the limit $R/\ell_-\to 0$, however, we find from Eq. (94) that the mobility in the co-rotating frame now vanishes logarithmically as it did for the sphere,

$$\lim_{R/\ell_- \to 0} \mu_{\theta,\mathrm{corot}} = \frac{1}{4\pi\eta_m}\left[\ln\left(\frac{R}{a}\right) - \frac{1}{2}\right]. \tag{102}$$

In Fig. 4, we plot the various mobilities for a pointlike particle embedded in a cylindrical membrane as a function of the dimensionless parameter R/ℓ_-, for various values of the viscosity of the external embedding fluid, i.e., ℓ_+. We can see that in all cases, the mobilities approach the flat-membrane mobility Eq. (49) for large R/ℓ_-. In addition, the mobilities display the expected asymptotic behavior in the limit of high curvature, R/ℓ_-.

For intermediate curvatures, the behavior of the cylindrical membrane mobilities is similar to the spherical membrane mobilities in many respects. For example, the mobility in the pinned cylindrical membrane $\mu_{\theta,\mathrm{pin}}$ displays a similar nonmonotonic dependence on R/ℓ_-, although this behavior is much more dramatic on the spherical membrane. This is due to the fact that the effects of the rigid rotational motion are much weaker in the cylindrical membrane than for the spherical membrane. As a result, the nonmonotonic behavior of μ_{pin} at intermediate curvatures—which, as argued above, arises because of this rotational motion—is much weaker. We can also see that the nature of the approach to the flat-space limit for the cylindrical membrane mobilities depends on the ratio of the fluid viscosities of the embedding fluids, as it does on the sphere. In particular, when $\eta_+ < \eta_-$ the mobility decreases from the flat-space limit much more quickly than when $\eta_+ > \eta_-$. Again, this effect is not as strong as it is in the spherical membrane case, where the mobilities approached the flat-space limit *from above* when $\eta_+ > \eta_-$: for the cylindrical membranes, this only occurs for $\mu_{\theta,\mathrm{pin}}$. This is not surprising: the geometric asymmetry between the two embedding fluids is much stronger in the spherical case than it is for the cylindrical case, since the interior fluid is bounded inside the sphere but unbounded inside the cylinder. As a result, the effects of asymmetry in the viscosities are much weaker for a cylindrical membrane.

VI. DISCUSSION

In this article, we have presented first an extended introduction to the hydrodynamics of flows on curved membranes and then two illustrative examples of the effects of curvature. These calculations were shown in sufficient detail to allow the interested reader to pursue analogous calculations for a variety of membrane shapes. We now summarize the principal results, discuss their significance, and propose experimental tests of this work.

We begin by making a few general points. The focus of our work is understanding the role of geometry in membrane hydrodynamics. There are two distinct geometric effects that must be accounted for in this system. The first is the effect of intrinsic Gaussian curvature on the in-plane membrane stresses. This result can best be seen in terms of the results of Sec. II. For the purposes of comparison, it may be recalled that in standard three-dimensional low Reynolds number hydrodynamics the velocity can be derived in terms of an axial vector potential that ensures the incompressibility of the flow. In addition, the velocity field itself must satisfy Laplace's equation. In Sec. II, Eq. (13) we compute the analogous equation of motion for the velocity field in membrane hydrodynamics. From this result, we note that there is now an additional source for the Laplacian and that geometry—specifically the Gaussian curvature of the membrane—is responsible for this term. Physically, the additional term can be understood by noting that, in the presence of Gaussian curvature, a spatially uniform flow field generates internal shear stresses in the membrane. These additional in-plane stresses arise entirely from the membrane's curvature without regard to the flows in the embedding fluids.

The difference between our results for the spherical membrane, which has a constant nonvanishing Gaussian curvature, and the cylindrical membrane, which has an everywhere zero Gaussian curvature, cannot be attributed solely to this effect. After all the flat membrane studied previously also has zero Gaussian curvature, but our results for particle mobilities on cylindrical and flat membranes differ dramatically. From a hydrodynamic perspective, there should be no difference between cylindrical and flat membranes in a vacuum (or in embedding fluids with vanishingly small viscosities). The remaining difference thus highlights the importance of the flows generated in the embedding fluids due to the flows in the membrane. The effect of geometry on membrane hydrodynamics thus has two distinct sources: the first is due to the alteration of the in-plane stresses by the Gaussian curvature; the second is caused by the geometric modification of nonlocal interactions between separate points on the membrane mediated by flows through the embedding fluids. If one were to solve the coupled hydrodynamic equations for a surface of arbitrary but fixed geometry (perhaps numerically), this distinction would still apply.

Another effect of nontrivial geometry is that it introduces length scales in addition to the SD length. In fact, our calculations suggest that membrane hydrodynamics in the presence of curvature generically admits three lengths: the mean curvature, and two SD lengths defined by the ratio of the membrane viscosity to the viscosities of the two embedding fluids. Of course, a flat membrane can also separate two distinct fluids of differing viscosities, but these two viscosities enter the SD length symmetrically in the form of their mean. This is the result of the reflection symmetry of the flat membrane system about its normal. Curvature breaks this symmetry, allowing the two viscosities to enter the solution in an asymmetric manner. This is best seen in Eq. (38), which gives the relative weighting of the various spherical harmonic modes of the velocity field in response to a point force on the sphere. The dependence of the amplitudes upon the viscosity of the interior fluid through ℓ_- vanishes for the $l=1$ mode, which corresponds to the rigid body rotation of the spherical membrane and the interior fluid. There is no analogous term in which the influence of the viscosity of the outer fluid (though ℓ_+) vanishes. A similar result can be seen for the cylindrical membrane in Eq. (81).

Comparing velocity fields on the membranes shown for the sphere in Fig. 1 and for the cylinder in Fig. 3, we observe a topologically determined effect. The motion of the particle always introduces a nonvanishing and continuous velocity vector field on the membrane. The Poincaré-Hopf theorem of

algebraic topology requires such a continuous vector field on a compact manifold to have topological defects whose charges sum to the Euler characteristic of the manifold [20]. For the sphere, the Euler characteristic is two. The vortices in the velocity field of Fig. 1 (one shown in the figure and one symmetrically placed on the other side of the sphere and not shown) are the charge one defects required to satisfy this theorem. The cylinder, on the other hand, has an Euler characteristic of zero and thus requires no such defects in the velocity generated on its surface by the motion of a particle, as shown in Fig. 3. If one uses the so-called unsteady Stokes approximation to examine time-dependent flows in three-dimensional hydrodynamics at low Reynolds number, one finds that vorticity obeys a diffusion equation [36]. When a particle is initially moved, vortices of opposite sign (i.e., sign of the curl of the velocity field) are generated at the particle and move outward with diffusive scaling. At long times, these vortices diffuse to infinity, leaving behind the vortex-free Stokes flow around the moving particle. On the spherical membrane these vortices remain in the *steady-state* flow, a dynamical consequence of the changed topology of the surface.

Determinations of a particle's mobility on a sphere presents a definitional ambiguity. One may define the mobility as usual by the ratio of the velocity of the particle to the applied force, but one must decide whether the contribution to the particle's velocity due to the rigid rotation of the entire sphere should be included. Doing so produces a large correction to the mobility when the sphere is small compared to the SD length. In that limit, the sphere rotates nearly as a rigid body. Rather than proscribe the correct definition, we presented three options including the naïve mobility that includes this free rotation effect. Another possible definition is the pinned mobility, in which we imagine the sphere to be pinned to a substrate at the antipode of the moving particle. This mobility provides the closest approximation to the experimental situations of which we are aware, but seems somewhat arbitrary. Alternatively, measuring the particle's velocity in a frame that co-rotates with rigid body motion of the sphere presents the most natural meaning of the mobility of particles within the spherical membrane. The calculations for the free mobility, pinned mobility, and co-rotating mobility are found in Eqs. (48), (55), and (57), respectively. Various limiting cases are discussed regarding these equations. In general these functions cannot be written simply in closed form, but the mobilities are plotted as a function of radius of the spherical membrane in Fig. 2.

On the cylinder, particulate mobilities are anisotropic and represented by a mobility tensor that has two independent components. For the mobility in the direction along the long axis of the cylinder, one can consider a single definition of mobility—the one in which the particle's velocity is measured in the rest frame of the cylinder. For the mobility in the orthogonal direction, one can define three mobilities in analogy those defined for the sphere. Although the infinite cylinder cannot rotate as a rigid body in response to a finite point force, the flow field around the particle approaches that of a locally rigid rotation. The mobilities for particle motion on a cylinder are given by Eqs. (89), (92), (100), and (101); they are plotted as a function of the radius of the cylinder in Fig. 4.

Preliminary experimental tests of these results have been performed by directly imaging the flow field around a rodlike particle moving on a spherical membrane [8]. Since it is possible to produce both spherical and cylindrical lipid bilayers [37], we believe that more detailed tests of particle mobilities on these surfaces can be performed using standard measurements of diffusion, such as fluorescence recovery after photobleaching or particle tracking. Such diffusion measurements indirectly measure the particle mobilities by the Stokes-Einstein relation. It is also possible to use particle tracking to directly measure the entire membrane velocity field around a driven particle, as was done in Ref. [8] for spherical interfaces. The same experiment should be possible for flow field on cylindrical tethers as well.

We have studied membrane hydrodynamics on surfaces having positive and zero Gaussian curvature. In order to more fully understand the role of Gaussian curvature, it seems reasonable to suggest that one should examine a surface of constant negative Gaussian curvature as well. While exotic surfaces of this sort do exist, e.g., the pseudosphere of Beltrami, these are not simply realized experimentally. Moreover finding analytic solutions for the hydrodynamic flows of the embedding fluid in this case is challenging. It may be possible to make progress on the measurement of particulate mobilities in the presence of negative Gaussian curvature by considering a catenoid—the minimal surface formed by a membrane supported by two coaxial rings. This surface, however, has a nonconstant but everywhere negative Gaussian curvature; the variation in the Gaussian curvature makes the eigenvalue problem associated with the solution of the in-plane flows difficult. The solution of the flows of the embedding fluids will also prove difficult. Along the same lines, one may examine topologically distinct surfaces that require changes in the number of topological defects in the membrane velocity field in order to test the importance of topological considerations for particulate mobilities.

Even for the two cases studied in detail here, one may extend our results to the case of unsteady flows. For example, how are the dynamics of the vortices associated with the initiation of flow changed by geometry? Finally, we point out that all of the calculations performed or proposed here assume a *fixed* membrane geometry and may be approached using the formalism discussed in this article, although we expect more complex membrane geometries will require numerical solutions to these equations. Membrane hydrodynamics on deformable membranes (having a dynamic local geometry) present a set of questions that cannot be addressed with the current theory.

[1] P. J. R. Spooner, R. H. E. Friesen, J. Knol, B. Poolman, and A. Watts, Biophys. J. **79**, 756 (2000).
[2] K. Simons and E. Ikonen, Nature (London) **387**, 569 (1997).
[3] S. L. Veatch and S. L. Keller, Phys. Rev. Lett. **94**, 148101 (2005).
[4] D. K. Schwartz, C. M. Knobler, and R. Bruinsma, Phys. Rev. Lett. **73**, 2841 (1994).
[5] H. A. Stone and A. Ajdari, J. Fluid Mech. **369**, 151 (1998).
[6] M. Sickert, F. Rondelez, and H. A. Stone, EPL **79**, 66005 (2007).
[7] V. Prasad, S. A. Koehler, and E. R. Weeks, Phys. Rev. Lett. **97**, 176001 (2006).
[8] M. L. Henle, R. McGorty, A. B. Schofield, A. D. Dinsmore, and A. J. Levine, EPL **84**, 48001 (2008).
[9] S. L. Veatch and S. L. Keller, Biochim. Biophys. Acta **1746**, 172 (2005).
[10] A. D. Dinsmore, M. F. Hsu, M. G. Nikolaides, M. Marquez, A. R. Bausch, and D. A. Weitz, Science **298**, 1006 (2002).
[11] B. Maier and J. O. Radler, Macromolecules **33**, 7185 (2000).
[12] P. G. Saffman and M. Delbrück, Proc. Natl. Acad. Sci. U.S.A. **72**, 3111 (1975).
[13] A. J. Levine and F. C. MacKintosh, Phys. Rev. E **66**, 061606 (2002).
[14] A. J. Levine, T. B. Liverpool, and F. C. MacKintosh, Phys. Rev. Lett. **93**, 038102 (2004).
[15] V. Prasad and E. R. Weeks, Phys. Rev. Lett. **102**, 178302 (2009).
[16] H. A. Stone, J. Fluid Mech. **409**, 165 (2000).
[17] A. Anguelouch, R. L. Leheny, and D. H. Reich, Appl. Phys. Lett. **89**, 111914 (2006).
[18] A. J. Levine, T. B. Liverpool, and F. C. MacKintosh, Phys. Rev. E **69**, 021503 (2004).
[19] D. R. Daniels and M. S. Turner, Langmuir **23**, 6667 (2007).
[20] T. Gamelin and R. Greene, *Introduction to Topology* (Dover Publications, New York, 1999).
[21] M. G. Munoz, L. Luna, F. Monroy, R. G. Rubio, and F. Ortega, Langmuir **16**, 6657 (2000).
[22] Y. Jayalakshmi, L. Ozanne, and D. Langevin, J. Colloid Interface Sci. **170**, 358 (1995).
[23] M. L. Kurnaz and D. K. Schwartz, Phys. Rev. E **56**, 3378 (1997).
[24] E. Helfer, S. Harlepp, L. Bourdieu, J. Robert, F. C. MacKintosh, and D. Chatenay, Phys. Rev. Lett. **85**, 457 (2000).
[25] E. Helfer, S. Harlepp, L. Bourdieu, J. Robert, F. C. MacKintosh, and D. Chatenay, Phys. Rev. E **63**, 021904 (2001).
[26] M. L. Henle and A. J. Levine, Phys. Fluids **21**, 033106 (2009).
[27] W. Cai and T. C. Lubensky, Phys. Rev. Lett. **73**, 1186 (1994).
[28] W. Cai and T. C. Lubensky, Phys. Rev. E **52**, 4251 (1995).
[29] U. Seifert, Eur. Phys. J. B **8**, 405 (1999).
[30] S. Ramaswamy, J. Prost, W. Cai, and T. C. Lubensky, EPL **23**, 271 (1993).
[31] S. Ramaswamy, J. Prost, and T. C. Lubensky, EPL **27**, 285 (1994).
[32] F. I. Niordson, *Shell Theory* (North-Holland, New York, 1985).
[33] E. Kreyszig, *Differential Geometry* (Dover Publications, New York, 1991).
[34] B. D. Hughes, B. A. Pailthorpe, and L. R. White, J. Fluid Mech. **110**, 349 (1981).
[35] J. Happel and H. Brenner, *Low Reynolds Number Hydrodynamics with Special Applications to Particulate Media* (Kluwer, The Netherlands, 1983).
[36] T. B. Liverpool and F. C. MacKintosh, Phys. Rev. Lett. **95**, 208303 (2005).
[37] T. R. Powers, G. Huber, and R. E. Goldstein, Phys. Rev. E **65**, 041901 (2002).
[38] This formula was misprinted in Ref. [8].